Nitrate Removal from Aqueous Solution Using Natural Zeolite-Supported Zero-Valent Iron Nanoparticles

Saloome SEPEHRI, Manoucher HEIDARPOUR and Jahangir ABEDI-KOUPAI

Department of Water Engineering, Isfahan University of Technology, Isfahan, Iran

Abstract

Sepehri S., Heidarpour M., Abedi-Koupai J. (2014): **Nitrate removal from aqueous solution using natural zeolite-supported zero-valent iron nanoparticles**. Soil & Water Res., **9**: 224–232.

A report on the synthesis and characterization of nanoscale zero-valent iron in the presence of natural zeolite as a stabilizer is presented. This novel adsorbent (Ze-nZVI) was synthesized by the sodium borohydride reduction method. The scanning electron microscopy (SEM) images revealed that the stabilized nZVI particles were uniformly dispersed across the zeolite surface without obvious aggregation. The synthesized Ze-nZVI material was then tested for the removal of nitrate from aqueous solution. The effect of various parameters on the removal process, such as initial concentration of nitrate, contact time, initial pH, and Ze-nZVI dosage, was studied. Batch experiments revealed that the supported nZVI materials generally have great flexibility and high activity for nitrate removal from aqueous solution. The nitrogen mass balance calculation showed that ammonium was the major product of nitrate reduction by Ze-nZVI (more than 84% of the nitrate reduced); subsequently the natural zeolite in Ze-nZVI removed it completely via adsorption. The kinetic experiments indicated that the removal of nitrate followed the pseudo-second-order kinetic model. The removal efficiency for nitrate decreased continuously with an increase in the initial solution pH value and Ze-nZVI dosage but increased with the increase in the initial concentration of nitrate. The overall results indicated the potential efficacy of Ze-nZVI for environmental remediation application.

Keywords: chemical reduction; kinetic modelling; nanoscale zero-valent iron particles; natural zeolite; nitrate; sorption isotherm

High nitrate concentration has become a serious common water quality problem in agricultural regions. In recent years, nanoscale zero-valent iron (nZVI) has been widely studied as an environmentally friendly strong reducing agent. Several studies reported the efficiency of nZVI for the removal of a variety of contaminants (Fu *et al.* 2014). However, nZVI particles expose vigorous propensity to agglomerate into larger solid particles. Moreover, the separation of non-supported nZVI particles from the aqueous phase is still a difficult task (Wang *et al.* 2008). The published results revealed that the presence of support materials leads to a decrease in the aggregation of nZVI and a corresponding increase in the Specific Surface Area (SSA) (Fu *et al.* 2014). Li *et al.* (2010) investigated Cr(VI) removal by montmorillonite (Mont) and hexadecyltrimethylammonium modified montmorillonite-supported iron nanoparticles (HDTMA-Mont). They reported that

SSAs for the Mont and HDTMA-Mont were 28.7 and 38.1 m^2/g, respectively, while for unsupported nZVI they were 24.3 m^2/g (Li *et al.* 2010).

Most researches on nitrate reduction using nZVI indicated that nitrite, nitrogen gas, and ammonium could be possible products of nitrate reduction, which might lead to further treatment requirements (Hwang *et al.* 2011). The main reaction approach shown in Eq. (1) is about the deoxidization of nitrate to ammonium.

$$4Fe^0 + NO_3^- + 10H^+ = 4Fe^{2+} + NH_4^+ + 3H_2O \qquad (1)$$
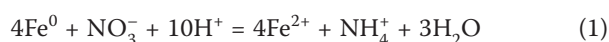
In this study, a synthesized natural zeolite-supported nanoscale zero-valent iron (Ze-nZVI) was proposed for the effective reduction of nitrate from the aqueous solution without ammonium release. This paper reports on the five following issues: (1) synthesis of Ze-nZVI and the characterization of the modi-

fied bead with scanning electron microscopy (SEM), powder X-ray diffraction (XRD), Fourier transform infrared spectroscopy (FTIR), and Brunauer-Emmett-Teller (BET-N_2) technology, (2) comparison of nitrate removal using Ze-nZVI and natural zeolite (Ze), (3) evaluation of the sorbent dosage, and initial pH effects on the removal process, (4) determination of the possible end-products of nitrate reduction using Ze-nZVI, and (5) kinetics and isotherm of nitrate adsorption by Ze-nZVI and Ze.

MATERIAL AND METHODS

Material and chemicals. The natural zeolite used in this study was obtained from Semnan province mines of volcanic tuffs, Iran. After drying at 60°C overnight, raw zeolite was ground and sieved with a 200 mesh screen prior to use. Cation exchange capacity (CEC) of Ze was measured using a 1M NH_4OAc saturation method (Chapman 1965).

Ferrous sulfate heptahydrate ($FeSO_4 \times 7H_2O$) and sodium borohydride ($NaBH_4$) were used as received (98% Aldrich, Aldrich, St. Louis, USA). The following chemicals were purchased from Merck (Darmstadt, Germany): ethanol (96%), NaOH (99%), HCl (98%), KCl (99%), and KNO_3 (98%).

Synthesis of Ze-nZVI. The synthesis of Ze-nZVI was based on the reduction of ferrous iron with borohydride, in which zeolite acted as a porous-based support material. This method originally reported on preparing nZVI from Fe^{2+} ions (Li *et al.* 2011b). A ferrous solution was produced by dissolving sulfate heptahydrate (6.51 g) in a 4/1 (v/v) ethanol/deionized water mixture (50 ml). This solution was initially placed into a three-necked open flask and then, to obtain Ze-nZVI with a zeolite/iron mass ratio 1:1, zeolite (1.31 g) was added to the flask and stirred for 30 min. Then, $NaBH_4$ (2.67 g) was dissolved in 80 ml of deionized water to provide 1M solution (BH_4^-/Fe^{2+} molar ratio of 3) and added drop-wise into the aqueous mixture with constant vigorous stirring under a N_2 atmosphere. Borohydride reduces Fe to ions based on the following reaction (Li *et al.* 2010):

$$Fe^{+2} + 2BH_4^- + 6H_2O \rightarrow Fe^0 + 2B(OH)_3 + 7H_2 \uparrow \qquad (2)$$
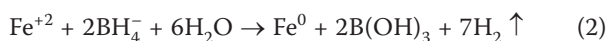
All parameters were considered constant during the experiment. The solution colour changed immediately to black, indicating the formation of supported nZVI. The formed black solid particles were separated by vacuum filtration using Whatman filter papers and rinsed quickly three times with ethanol. Ze-nZVI samples were dried at 75°C under vacuum overnight and kept under the N_2 atmosphere prior to use (Üzüm *et al.* 2009).

Characterization and measurements. Total elemental analysis of Ze was performed by a Spectro X-Lab 2000 (Bruker, Kalkar, Germany) X-Ray Fuorescence (XRF) spectrometer. SEM characterization was performed by Hitachi S-4160 instrument (20 kV) (Hitachi, Tokyo, Japan). SSAs of Ze and Ze-nZVI samples were determined by BET-N_2 method using a BELSORP mini II (BelJapan, Osaka, Japan) instrument. XRD measurements of Ze and Ze-nZVI were carried out using Philips X'PERT MPD diffractometer (Cu-Kα radiation, λ = 1.54 Å, scan rate: 0.05°/s) (Philips, Eindhoven, Netherlands). FTIR spectra for Ze and Ze-nZVI were obtained with a Fourier transform infrared spectroscope FTIR Tensor 27 (Bruker) at room temperature. The concentration of nitrate and nitrite in solution was analyzed based on the guidelines given in the 20th edition of the standard methods by means of a UV/Vis spectrophotometer (model V-530) (APHA 1992). At the end of the reaction, the mass of ammonium sorbed on Ze-nZVI was measured by extracting with 1M KCl solution and analyzing the extract solution. NH_4^+ was analyzed by a steam distillation procedure (Keeney & Nelson 1982).

Batch experiments. To evaluate the efficiency of Ze-nZVI and Ze for the nitrate removal in the aqueous solution, experiments were conducted. The aqueous nitrate solutions were prepared by dissolving appropriate amounts of KNO_3 in distilled deionized water. The effects of sorbent dosage and initial pH on the removal process were investigated. In addition, kinetics and equilibrium isotherm studies were performed with different initial concentrations of nitrate. The batch experiments were carried out in 50 ml polyethylene bottles containing 0.1 g Ze-nZVI and Ze and 10 ml of nitrate solutions of desired concentrations and pH. All tests were performed in triplicate. The solutions were mixed in a shaker with an agitation speed of 200 rpm. At the end of the reaction period, each sample was filtered and the nitrate concentration in the supernatant was analyzed immediately. The removal efficiency and the adsorption capacity (q_e, mg/g) of sorbents were calculated as follows:

$$\text{Removal (\%)} = \frac{C_0 - C_e}{C_0} \times 100 \qquad (3)$$

$$q_e = \frac{(C_0 - C_e) \times V}{m} \qquad (4)$$

where:

C_0, C_e – concentrations of nitrate at initial and equilibrium (mg/l)

m – mass of sorbent (g)

V – volume of the solution (l)

RESULTS AND DISCUSSION

Characterization of Ze and Ze-nZVI. The chemical composition (%) of Ze determined by XRF method was: 62.7 SiO_2, 10.8 Al_2O_3, 5.8 Na_2O, 2.4 K_2O, 2.7 CaO, 1.05 Fe_2O_3, 0.7 MgO, 0.14 TiO_2, 0.01 P_2O_5, and 13.2 Loss of Ignition (LOI). CEC of Ze was 135 (cmol/kg). SSAs for Ze-nZVI and Ze measured by BET-N_2 method were 49.7 and 17.8 m^2/g, respectively. The XRD patterns of Ze and Ze-nZVI before and after reacting with nitrate are shown in Figure 1.

The strong peaks at 22.2, 25, 26, 28.1, and 31.9 Å indicated a high percentage of clinoptilolite mineral in the sample (Figure 1a). The XRD pattern of Ze-nZVI before reacting with nitrate (Figure 1b) displayed obvious peaks of Fe^0 (b1: 2θ = 44.8, b2: 2θ = 65.1) and confirmed its existence in freshly prepared Ze-nZVI (Üzüm *et al.* 2009). The weak peak at 2θ = 52.9 corresponds to goethite. The Ze-nZVI had a typical clinoptilolite zeolite structure. It was emphasized that the zeolite framework and the total crystalline structure were not noticeably changed after stabilizing Fe^0 nanoparticles. Thus, Fe^0 nanoparticles may be stabilized on the external surface of zeolite. XRD-based evaluations of the particle size indicated the size of about 40 nm based on the Debye-Scherrer method (Birks & Friedman 1946). The comparison between XRD patterns of Ze-nZVI before and after reacting with nitrate indicated that Fe^0 peaks were weakened significantly. Moreover, the peaks at 2θ = 35.4, 35.6, and 60.5 (c1, c2, and c3; Figure 1c) represented the characteristic peaks of magnetite, hematite, and maghemite, respectively, and indicated that iron oxide layers were formed. It is evident that nZVI were acting as reducing agents and redox reaction occurred between Fe^0 and nitrate ions.
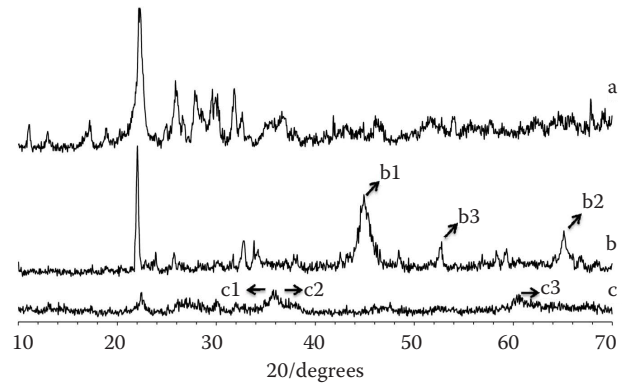

Figure 1. XRD patterns of (a) Ze; (b) Ze-nZVI before reacting with nitrate; (c) Ze-nZVI after reacting with nitrate b1 (2θ = 44.8) and b2 (2θ = 65.1): Fe^0; b3: goethite (α-FeOOH, 2θ = 52.9); c1: magnetite (Fe_3O_4, 2θ = 35.4); c2: hematite (α-Fe_2O_3, 2θ = 35.6); c3: maghemite (γ-Fe_2O_3, 2θ = 60.5)

In Figure 2a showing the Ze morphology it can be observed that Ze is in the form of euhedral plates, laths, and smooth layers. As shown in Figure 2b, the stabilized nZVI particles had the core-shell structure and were widely dispersed across the zeolite surface without obvious aggregation.

Fe^{2+} was adsorbed on the surface of zeolite by ion-exchange reaction. These exchanged Fe^{2+} ions were reduced to Fe^0 with $NaBH_4$, which resulted in good dispersed nZVI on the zeolite surface. Similar results have been reported using bentonite and kaolinite supported iron nanoparticles (Üzüm *et al.* 2009; Shi *et al.* 2011). Measuring the diameters of 100 particles in different regions of a given image grid can be used to quantify the particle size (Wang *et al.* 2010). The average particle size calculated based on this method was 45 nm, which is in a good agreement with the size determined by the XRD pattern. Analysis of the SEM image of nZVI particles after reacting with nitrate (Figure 2c) indicated the formation of nearly rectangular particles with larger size compared to nZVI particles before reacting with nitrate (Tiraferri *et al.* 2008). This feature
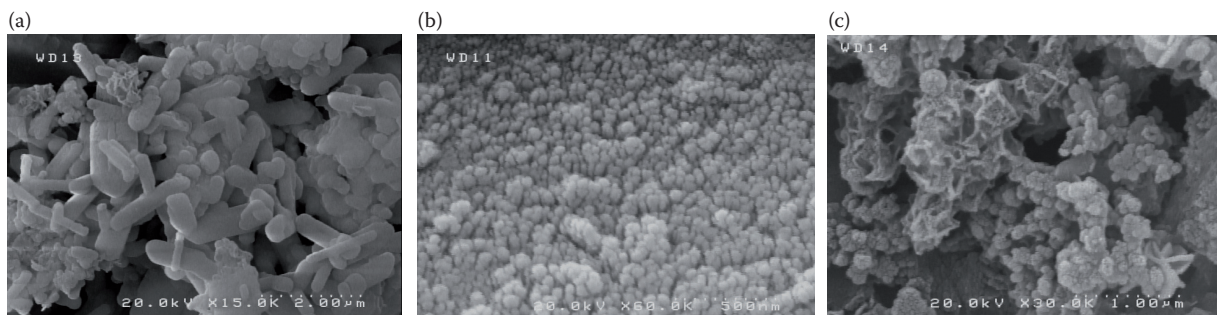

Figure 2. SEM images of Ze (a), Ze-nZVI before reacting with nitrate (b), and Ze-nZVI after reacting with nitrate (c)
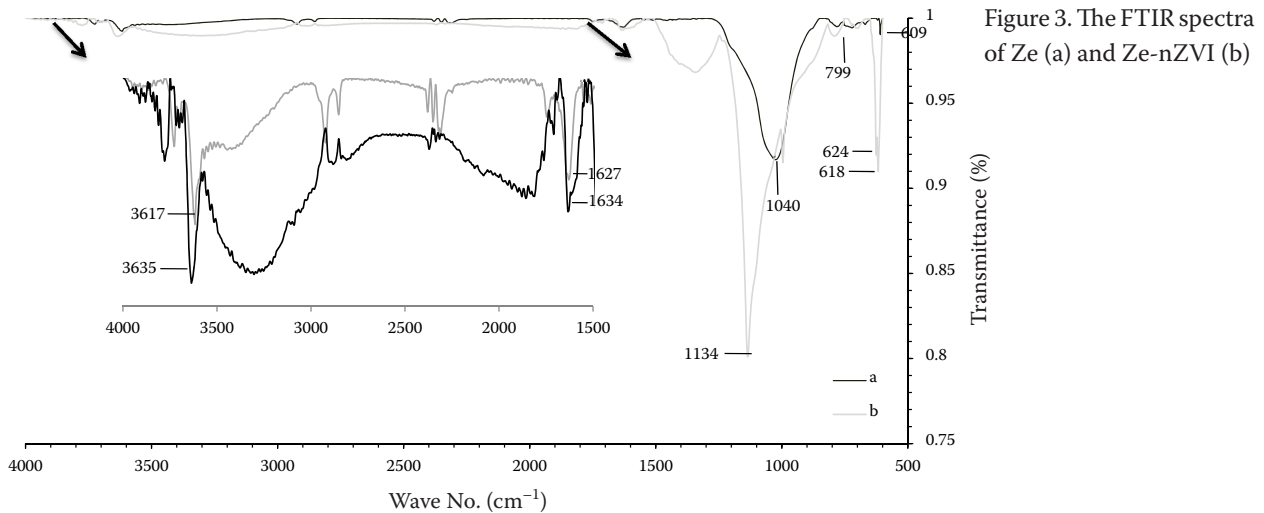
Figure 3. The FTIR spectra of Ze (a) and Ze-nZVI (b)

indicates that redox reaction occurred between Fe^0 and nitrate ions and as a result different types of iron (hydr)oxides were formed and consequently the particle size was increased (90 nm).

The FTIR spectra for Ze and Ze-nZVI (Figure 3) were obtained in the range of 500–4000 cm^{-1}. The strong bands at 1040 cm^{-1} (Figure 3a) and 1134 cm^{-1} (Figure 3b) can be assigned to the external vibrations between the (Al, Si)O_4 tetrahedrons. The 609 cm^{-1} (Figure 3a) and 618 cm^{-1} (Figure 3b) peaks are the typical clinoptilolite bands (Pechar & Rykl 1981). In accordance with achievements by Gotic & Music (2007), the IR band at 624 cm^{-1} is related to Fe-O stretching vibrations, also the weak band at 799 cm^{-1} appeared due to Fe-O-H bending vibrations in goethite (Figure 3b)(Gotic & Music 2007). These peaks were only identified in the spectrum of Ze-nZVI, which agreed well with the XRD pattern (Figure 1b). The effect of the stabilization of nZVI on Ze was observed with the shift in the wave numbers of the IR bands. On the basis of IR bands, the positions of the vibrations at 1627 and 3617 cm^{-1} (Figure 3a) (the stretching vibrations of the hydroxyl group) are very sensitive to the stabilization of nZVI and these bands are shifted to 1634 and 3635 cm^{-1} (Figure 3b), respectively. These results are similar to those obtained by other authors (Li *et al.* 2010, 2011a; Chen *et al.* 2011).

Effect of the initial pH. The effect of pH on the nitrate removal by Ze and Ze-nZVI was studied over a pH range of 2–10 with different initial concentrations of nitrate (30–200 mg/l) at 25°C (Ze and Ze-nZVI dosage = 10 g/l). As shown in Figure 4, the nitrate removal was highly dependent on the initial pH of the solution.

In the case of Ze-nZVI, the increase in H^+ concentration promoted the electron transfer between nZVI and nitrate ions, and consequently can prevent the formation of Fe(II) and Fe(III) precipitate on the surface of nZVI (Liu *et al.* 2012).

Effect of Ze and Ze-nZVI dosage. The initial loadings of Ze and Ze-nZVI in the nitrate solution (C_0 = 100 mg/l) were 2–10 g/l at initial pH = 5.5. It is observed that the increase in the sorbent dosage causes a noticeable increase in the removal efficiency (Figure 5). The nitrate removal (%) is increased rapidly from 56.6 to 74.2% for Ze-nZVI. These phenomena
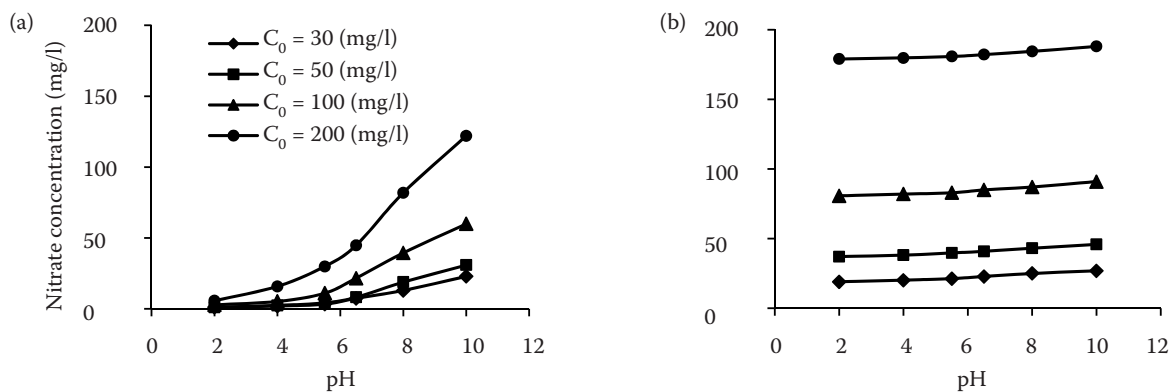

Figure 4. Effect of pH on the nitrate removal by Ze (a) and Ze-nZVI (b) at different initial nitrate concentrations
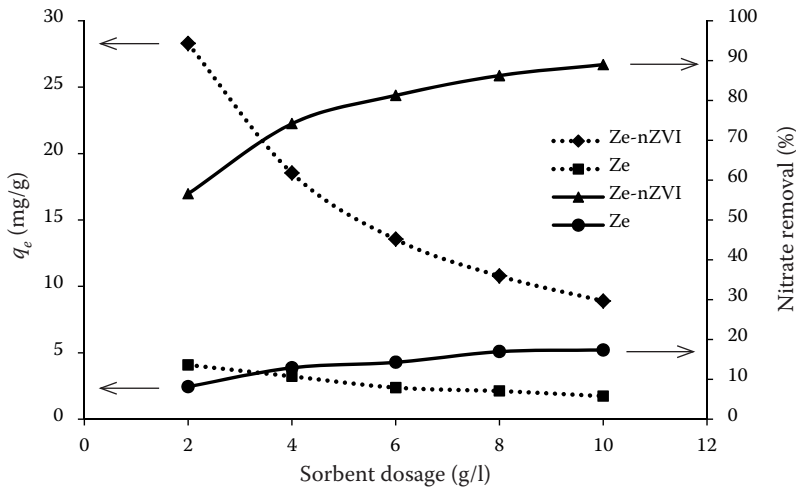
Figure 5. Effect of Ze and Ze-nZVI dosage on the nitrate removal at: C_0 = 100 mg/l, pH = 5.5, T = 25°C

can be attributed to the increase in the available active sites and larger surface area with the increase in the Ze-nZVI dosage (Huan *et al.* 2006; Shi *et al.* 2011).

Fate of nitrogen species during nitrate reduction by Ze-nZVI. In the experiments with Ze-nZVI, the concentration of ammonium, nitrite, and nitrate that accumulated in the solution at every time interval, was determined at initial pH = 5.5, 25°C, and C_0 = 100 mg/l. Moreover, the mass of ammonium sorbed on Ze-nZVI was measured by extracting with 1M KCl solution and analyzing the extract solution. The concentration of nitrogen species during nitrate reduction by Ze-nZVI is presented in Figure 6. The NH_4^+ concentration in the solution was undetectable at every time interval, indicating that the ammonium produced from nitrate reduction completely sorbed on Ze-nZVI. At the end of the reaction period, the NH_4^+-N concentration extracted from Ze-nZVI accounted for about 84.3% of the nitrate reduced (Figure 6). The total amount of nitrogen species (TN) in Ze-nZVI system was calculated as the sum of two main aqueous nitrogen species (nitrate and nitrite) and NH_4^+

extracted from Ze-nZVI, after the reduction reaction carried out for 24 h. The TN decreased to 14.5% of initial concentration. This phenomenon is probably due to the nitrogen conversion from aqueous phase to gas phase (nitrogen gas). This result agreed with the results of other researchers (Hwang *et al.* 2011; Shi *et al.* 2013). Hwang *et al.* (2011) proved that the role of nZVI in the removal of nitrate can be considered into two aspects: (*I*) adsorption of nitrate on the nZVI surface; (*II*) direct participation in the redox reaction (Hwang *et al.* 2011).

This result is pointed out by several authors for the removal of a variety of contaminants using nZVI including: Cr(VI) (Sherman *et al.* 2000; Geng *et al.* 2009), Pb^{2+} (Sherman *et al.* 2000), As(III) (Zhu *et al.* 2009; Horzum *et al.* 2013), NO_3^- (Rodríguez *et al.* 2009; Hwang *et al.* 2011), Cu^{2+}, Co^{2+} (Üzüm *et al.* 2009), pentachlorophenol (Li *et al.* 2011b), and methyl orange (Chen *et al.* 2011). As shown in Figure 6, there is an initial sorption phase during which the nitrate disappears from the solution significantly faster than in later phases. The kinetic
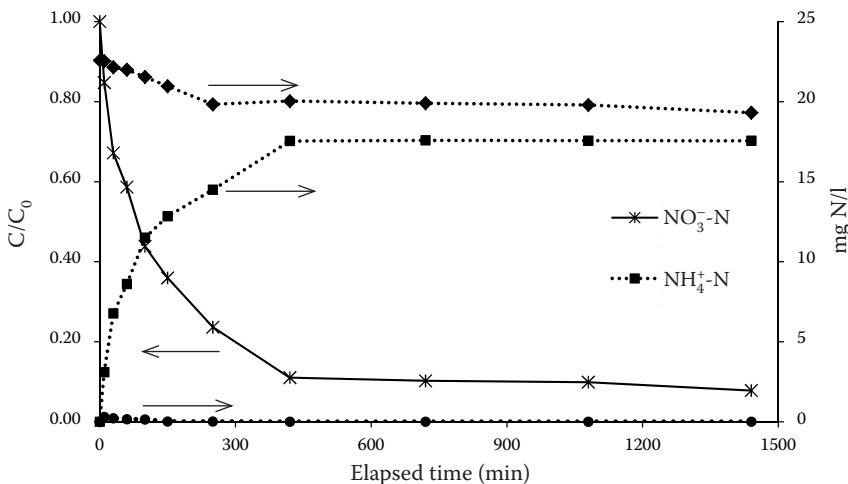

Figure 6. Total nitrogen, nitrate, and nitrite concentrations in residual solution and ammonium extracted from Ze-nZVI after reaction at: C_0 = 100 mg/l, pH = 5.5, T = 25°C

Table 1. Kinetic and isotherm equations

Model	Equation	No.
Pseudo-first-order	$q_t = q_e(1 - e^{-klt})$	(5)
Pseudo-second-order	$q_t = \dfrac{k_2 q_e^2 t}{1 + k_2 q_e}$	(6)
Elovich	$q_t = \left(\dfrac{1}{\beta}\right)\ln(\alpha\beta) + \left(\dfrac{1}{\beta}\right)\ln t$	(7)
Langmuir	$q_e = \dfrac{q_m K_l C_e}{1 + K_l C_e}$	(8)
Freundlich	$q_e = k_F C_e^n$	(9)
Redlich-Peterson	$q_e = \dfrac{a C_e}{1 + b C_e^n}$	(10)

q_t (mg/g) – amount of the nitrate removed per unit mass of sorbent at any time t (min); q_m – the maximum adsorption capacity of the adsorbent (mg/g); q_e – adsorption capacity (mg/g), k_1, k_2, α, β, K_l (l/mg), k_F (l/g), n, a, b – constants

and equilibrium isotherms of nitrate adsorption using Ze-nZVI are described in the next section.

Kinetic and isotherm equilibrium. The adsorption rate of nitrate was studied at initial pH = 5.5 and 25°C us-ing two initial nitrate concentrations (50 and 100 mg/l) up to a contact time of 24 h. The experimental results were fitted to the kinetic models of pseudo-first-order, pseudo- second-order, and Elovich (Qiu *et al.* 2009) defined in Eqs. (5), (7) (Table 1).

Moreover, the isotherm equilibrium experiments were performed using different concentrations of the nitrate solutions (20–320 mg/l) with the initial pH = 5.5 and temperature of 25°C. The equilibrium adsorption data were fitted to isotherm models of Langmuir, Freundlich, and Redlich-Peterson (Foo & Hameed 2010) defined in Eqs. (8)–(10) (Table 1).

The conformity between experimental results and the models-predicted values was expressed by nonlin-ear regression analysis using GraphPad Prism (Version 5.04, 2010) tool. The application of the kinetic models on the experimental results is presented in Figures 7 and 8. Figure 9 indicates the isotherm plots for the adsorption of nitrate onto sorbents. Kinetic and isotherm models parameters for the removal of nitrate by sorbents, the correlation coefficients (R^2), and the standard error of estimate (SEE) values based on different models are summarized in Tables 2 and 3, respectively.
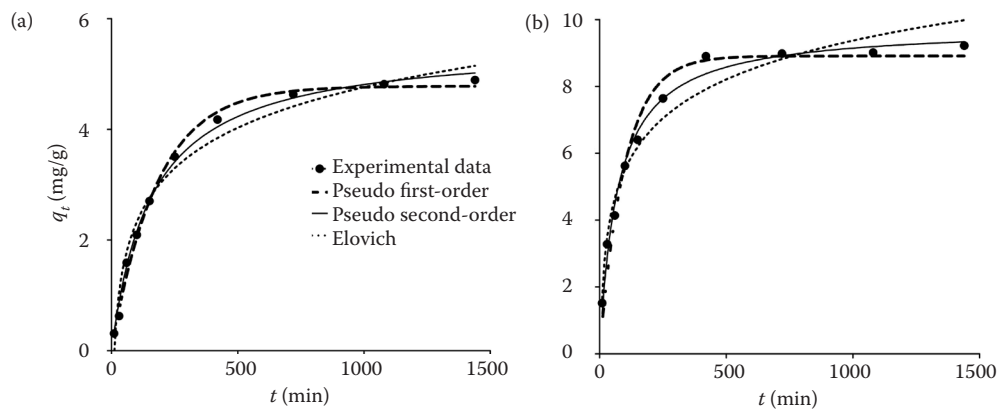

Figure 7. Kinetic plots for the adsorption of nitrate onto Ze-nZVI, $C_0 = 50$ (a), and $C_0 = 100$ (b) (mg/l)
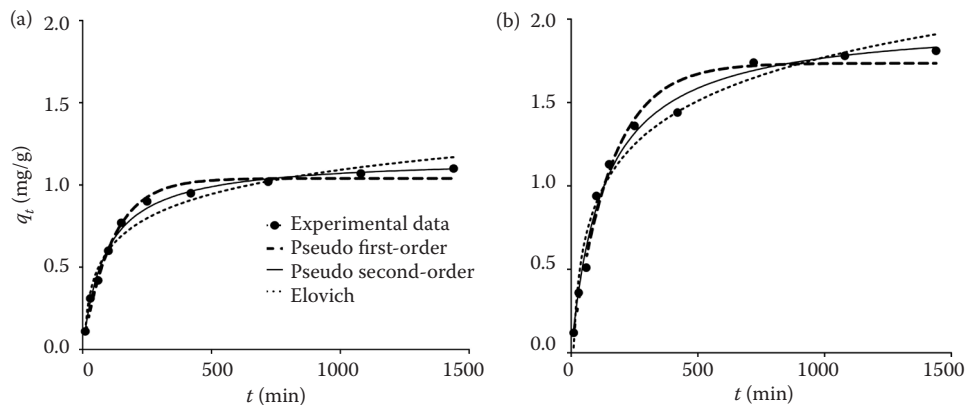

Figure 8. Kinetic plots for the adsorption of nitrate onto Ze, $C_0 = 50$ (a) and $C_0 = 100$ (b) (mg/l)

Table 2. Kinetic parameters for the adsorption of nitrate onto Ze and Ze-nZVI (in mg/l)

Model		Adsorbent			
		Ze		Ze-nZVI	
		$C_0 = 50$	$C_0 = 100$	$C_0 = 50$	$C_0 = 100$
q_e (exp) (mg/g)		1.10	1.81	4.90	9.22
Pseudo-first-order	q_e (mg/g)	1.04	1.74	4.51	8.91
	k_1 (l/mg)	0.009	0.007	0.006	0.01
	R^2	0.986	0.98	0.995	0.97
	SEE	0.04	0.09	0.12	0.51
Pseudo-second-order	q_e (mg/g)	1.166	1.996	5.272	9.790
	k_2 (l/mg)	0.01	0.004	0.001	0.0014
	R^2	0.994	0.99	0.9954	0.99
	SEE	0.03	0.07	0.12	0.31
Elovich	α	0.04	0.04	0.10	0.45
	β	4.71	2.65	0.95	0.60
	R^2	0.97	0.97	0.97	0.96
	SEE	0.06	0.11	0.30	0.56

C_0 –concentrations of nitrate at initial; q_e – adsorption capacity; R^2 – correlation coefficient; SEE – standard error of estimate; k_1, k_2, α, β – constants

In all cases, R^2 values for the pseudo-second-order kinetic model are higher than for the other kinetic models (Table 2). The equilibrium adsorption capacity is increased when the initial nitrate concentration is increased, but the essential time to reach equilibrium is independent of the initial nitrate concentration (Chatterjee & Woo 2009). The adsorption process reached equilibrium after about 12 and 7 h for Ze and Ze-nZVI, respectively. Moreover, it was found that the variations of the rate constant (k_2) have a decreasing trend when the initial nitrate concentration is increased.

Comparing R^2 values (Table 3) revealed that the experimental data were well fitted to the Langmuir model. This means that sorption takes place at the functional group/binding sites on the surface of the sorbents. Figure 9 illustrates that the nitrate adsorption capacity of Ze and Ze-nZVI is firstly increased
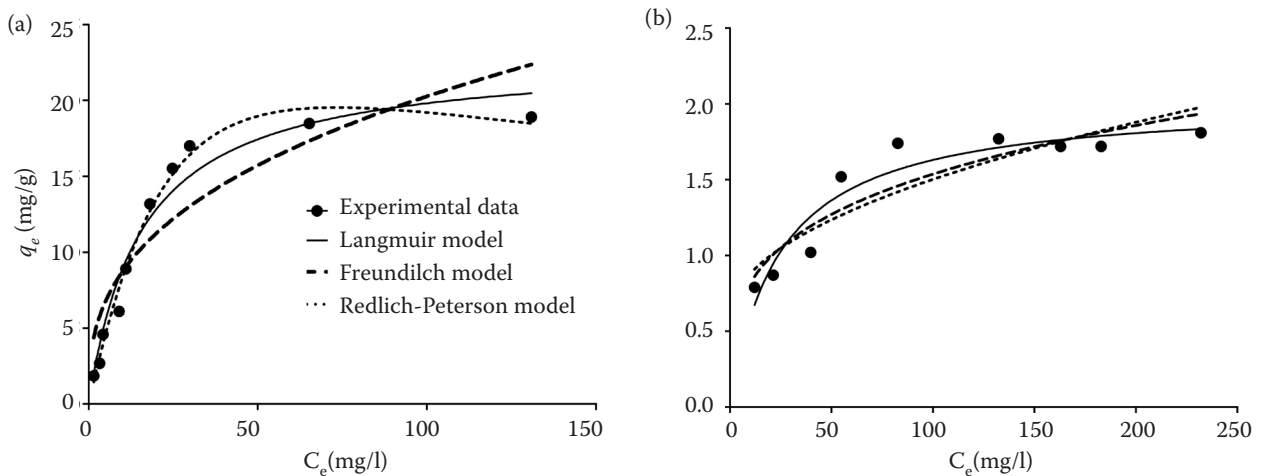

Figure 9. Isotherm plots for the adsorption of nitrate onto Ze-nZVI (a) and Ze (b)

Table 3. Isotherm parameters for the adsorption of nitrate onto Ze and Ze-nZVI

Isotherm		Adsorbent	
		Ze	Ze-nZVI
Langmuir	q_m (mg/g)	2.03	22.94
	k_l (l/mg)	0.04	0.06
	R^2	0.912	0.99
	SEE	0.14	0.44
Freundlich	k_f (l/mg)	0.44	3.75
	n	3.65	2.73
	R^2	0.85	0.82
	SEE	0.18	0.97
Redlich-Peterson	a	0.07	0.97
	b	0.02	0.01
	n	1.10	1.38
	R^2	0.91	0.96
	SEE	0.1	0.85

q_m – maximum adsorption capacity; R^2 – correlation coefficient; SEE – standard error of estimate; k_l, k_f, n, a, b – constants

with increasing the initial concentration of nitrate, and then it is not changed significantly, indicating that no more sites remain available for adsorption. The maximum adsorption capacities of Ze and Ze-nZVI for nitrate ions are 2.03 and 22.94 mg/g, respectively.

CONCLUSION

In this study, nZVI particles supported on natural zeolite clinoptilolite were synthesized, characterized, and applied in the removal of nitrate as a model contaminant from aqueous solution. This novel material has a high specific surface area and nZVI particles of 45 nm on the average are uniformly dispersed across the Ze surface without noticeable aggregation. Natural zeolite is a low-cost clay mineral, thus, this material could be an effective and promising stabilizer and dispersant for supporting nZVI due to its porous structure. Batch experiments indicated that the adsorption capacity decreased with increasing Ze-nZVI dosage and initial pH but increased with the increase in the initial concentration of nitrate. Reduction of nitrate using Ze-nZVI was in accordance with the pseudo-second-order kinetic model. Moreover, the equilibrium data were fitted well to the Langmuir model. The nitrogen mass balance calculation showed that nZVI particles in Ze-nZVI could generally reduce nitrate into ammonium (more than 84% of the nitrate reduced) and

nitrite usually occurs as intermediate. Subsequently, natural zeolite in Ze-nZVI absorbs unwanted ammonium completely due to its high selectivity for cations.

It could be concluded that nitrate removal using Ze-nZVI consists of three steps: (1) adsorption of nitrate on the nZVI surface; (2) redox reaction between nZVI and nitrate ions; (3) ammonium absorption by zeolite.

References

APHA (1992): Standard Methods for the Examination of Water and Wastewater. American Public Health Association, Washington, DC.

Birks L.S. Friedman H. (1946): Particle size determination from X-ray line broadening. Journal of Applied Physics, **16**: 687–692.

Chapman H.D. (1965): Cation Exchange Capacity. Method of Soil Analysis. SSAA, Madison.

Chatterjee S., Woo S.H. (2009): The removal of nitrate from aqueous solutions by chitosan hydrogel beads. Journal of Hazardous Materials, **164**: 1012–1018.

Chen Z.X., Jin X.Y., Chen Z., Megharaj M. (2011): Removal of methyl orange from aqueous solution using bentonite-supported nanoscale zero-valent iron. Journal of Colloid and Interface Science, **363**: 601–607.

Foo K.Y., Hameed B. (2010): Insights into the modeling of adsorption isotherm systems. Chemical Engineering Journal, **156**: 2–10.

Fu F., Dionysios D., Liu H. (2014): The use of zero-valent iron for groundwater remediation and wastewater treatment: A review. Journal of Hazardous Materials, http://dx.doi.org/10.1016/j.jhazmat.2013.12.062. (in print)

Geng B., Jin Z., Li T., Qi X. (2009): Preparation of chitosan-stabilized Fe^0 nanoparticles for removal of hexavalent chromium in water. Science of the Total Environment, **407**: 4994–5000.

Gotic M., Music S. (2007): Mossbauer, FTIR and FESEM investigation of iron oxides precipitated from $FeSo_4$ solutions. Journal of Molecular Structure, **834**: 445–453.

Horzum N., Demir M., Nairat M., Shahwan T. (2013): Chitosan fiber-supported zero-valent iron nanoparticles as a novel sorbent for sequestration of inorganic arsenic. RSC Advances, **3**: 7828–7837.

Huan Z., Zhao J., Lu H., Cheng Q. (2006): Synthesis of nanoscale zero-valent iron supported on exfoliated graphite for removal of nitrate. Transactions of Nonferrous Metals Society of China, **16**: 345–349.

Hwang Y.H., Kim D., Shin H. (2011): Mechanism study of nitrate reduction by nano zero valent iron. Journal of Hazardous Materials, **185**: 1513–1521.

Keeney D.R., Nelson D. (1982): Nitrogen Inorganic Forms. Methods of Soil Analysis. Part 2. 2nd Ed. Agronomy ASA, SSSA. Madison, 643–698.

Li S., Wu P., Li H., Zhu N., Li P., Wu J., Wang X., Dang Z. (2010): Synthesis and characterization of organo-montmorillonite supported iron nanoparticles. Applied Clay Science, **50**: 330–338.

Li Y., Li T., Jin Z. (2011a): Stabilization of Fe^0 nanoparticles with silica fume for enhanced transport and remediation of hexavalent chromium in water and soil. Journal of Environmental Sciences, **23**: 1211–1218.

Li Y., Zhang Y., Li J., Zheng X. (2011b): Enhanced removal of pentachlorophenol by a novel composite: Nanoscale zero valent iron immobilized on bentonite. Environmental Pollution, **159**: 3744–3749.

Liu T., Wang Z.L., Zhao L., Yang X. (2012): Enhanced chitosan/Fe^0-nanoparticles beads for hexavalent chromium removal from wastewater. Chemical Engineering Journal, **189**–**190**: 196–202.

Pechar F., Rykl D. (1981): Infrared spectra of natural zeolites of the stilbite group. Chemical Papers, **35**: 189–202.

Qiu H., Lv L., Pan B., Zhang Q., Zhang W., Zhang Q. (2009): Critical review in adsorption kinetic models. Journal of Zhejiang University Science, **10**: 716–724.

Rodríguez J.M., García F., García A., Gómez C., Vereda C. (2009): Kinetics of the chemical reduction of nitrate by zero-valent iron. Chemosphere, **74**: 804–809.

Sherman M., Ponder J., Darab G., Thomas E., Mallouk E. (2000): Remediation of Cr(VI) and Pb(II) aqueous solutions using supported, nanoscale zero-valent iron. Environmental Science & Technology, **34**: 2564–4569.

Shi J., Yi S., He H., Lomg C., Li A. (2013): Preparation of nanoscale zero-valent iron supported on chelating resin with nitrogen donor atoms for simultaneous reduction of Pb^{2+} and NO_3^-. Chemical Engineering Journal, **230**: 166–171.

Shi L., Zhang X., Chen Z. (2011): Removal of Cr(VI) from wastewater using bentonite-supported nanoscale zero-valent iron. Water Research, **45**: 886–892.

Tiraferri A., Chen K., Sethi R., Elimelech M. (2008): Reduced aggregation and sedimentation of zero-valent iron nanoparticles in the presence of guar gum. Journal of Colloid and Interface Science, **324**: 71–79.

Üzüm C., Shahwan T., Eroglu A., Hallam K., Scott T. (2009): Synthesis and characterization of kaolinite-supported zero-valent iron nanoparticles and their application for the removal of aqueous Cu^{2+} and Co^{2+} ions. Applied Clay Science, **43**: 172–181.

Wang W., Zhou M., Mao Q., Yue J., Wang X. (2010): Novel NaY zeolite-supported nanoscale zero-valent iron as an efficient heterogeneous fenton catalyst. Catalysis Communications, **11**: 937–941.

Wang X., Chen C., Liu H., Ma J. (2008): Preparation and characterization of PAA/PVDF membrane-immobilized Pd/Fe nanoparticles for dechlorination of trichloroacetic acid. Water Research, **42**: 4656–4664.

Zhu H., Jia Y., Wu J., Wang H. (2009): Removal of arsenic from water by supported nano zero-valent iron on activated carbon. Journal of Hazardous Materials, **172**: 1591–1596.

Corresponding author:

Saloome Sepehri, Isfahan University of Technology, Department of Water Engineering, P.O. Box 84156-83111, Isfahan, Iran; e-mail: s.sepehri@ag.iut.ac.ir